materials

MDPI

Article

Phase Formation Behavior and Thermoelectric Transport Properties of *P*-Type $Yb_xFe_3CoSb_{12}$ Prepared by Melt Spinning and Spark Plasma Sintering

Kyu Hyoung Lee [1], Sang Hyun Bae [2] and Soon-Mok Choi [2,*]

[1] Department of Materials Science and Engineering, Yonsei University, Seoul 03722, Korea; khlee2018@yonsei.ac.kr

[2] School of Energy, Materials and Chemical Engineering, Korea University of Technology and Education, Cheonan 31253, Korea; khansh@koreatech.ac.kr

* Correspondence: smchoi@koreatech.ac.kr

Received: 21 November 2019; Accepted: 20 December 2019; Published: 23 December 2019

Abstract: Formation of multiple phases is considered an effective approach for enhancing the performance of thermoelectric materials since it can reduce the thermal conductivity and improve the power factor. Herein, we report the in-situ generation of a submicron-scale (~500 nm) heterograin structure in *p*-type Yb-filled $(Fe,Co)_4Sb_{12}$ skutterudites during the melt spinning process. Mixed grains of $Yb_xFe_{3-y}Co_{1+y}Sb_{12}$ and $Yb_zFe_{3+y}Co_{1-y}Sb_{12}$ were formed in melt spun ribbons due to uneven distribution of cations. By the formation of interfaces between two different grains, the power factor was enhanced due to the formation of an energy barrier for carrier transport, and simultaneously the lattice thermal conductivity was reduced due to the intensified boundary phonon scattering. A high thermoelectric figure of merit *z*T of 0.66 was obtained at 700 K.

Keywords: multiple phases; thermoelectric; skutterudite; melt spinning; heterograin

1. Introduction

Skutterudite-based compounds such as *n*-type Co_4Sb_{12}-based and *p*-type $(Fe,Co)_4Sb_{12}$-based alloys are promising candidates for medium-high temperature (hot side temperature T_{hot} ~ 500 °C) thermoelectric (TE) power generation applications [1–3]. The maximum efficiency (η_{max}) of a TE power generation system is expressed by the following Equation (1):

$$\eta_{max} = \left[\frac{T_H - T_C}{T_H}\right]\left[\frac{\left(1+zT_{avg}\right)^{1/2}-1}{\left(1+zT_{avg}\right)^{1/2}+(T_C/T_H)}\right], \quad (1)$$

where T_H and T_C are the hot side temperature and cold side temperature of TE legs (*p*- and *n*-type TE materials in module), and zT_{avg} is the optimum dimensionless figure of merit zT ($= S^2\sigma T/\kappa$, where S is the Seebeck coefficient, σ is the electrical conductivity, and κ is the total thermal conductivity at a given absolute temperature T) value of the TE legs at average temperature ($T_{avg} = (T_H + T_C)/2$). Thus the development of skutterudites with a high zT is a prerequisite to realize a highly-efficient medium-high temperature TE power generation system with economic feasibility.

One of the most effective approaches to enhance the zT of skutterudites is the introduction of filler atoms including alkali, alkaline earth, and rare earth metals in nanocages of the lattice, which triggers a rattling effect to intensify high-frequency phonon scattering. Significantly reduced lattice thermal conductivity ($\kappa_{lat} = \kappa - \kappa_{ele}$, where κ_{ele} is the electronic contribution of thermal conduction)

was obtained both in *n*-type and *p*-type skutterudites [1,4]. Recently, based on the resonant scattering concept [5], multiple-filled skutterudites with an enhanced zT over 1.4 have been developed [6,7]. Together with the filling approach, formation of multiple phases beyond the grain size reduction is commonly employed since this approach can reduce the κ_{lat} and/or improve the power factor ($S^2\sigma$) [8]. The zT of TE materials with multiple phases is not determined by the average transport properties of the individual phases. Various interfacial effects such as carrier filtering and boundary phonon scattering to explain zT enhancement have been proposed [6–9]. Introducing nanoparticles into the skutterudite matrix is one of the simplest routes to form materials with multiple phases, whereby a reduced κ_{lat} is obtained while maintaining the power factor of the skutterudite matrix [10,11]. However, a well-controlled fabrication process for uniform dispersion of nanoparticles in the skutterudite matrix is always required to secure the enhancement of zT.

The second technology to generate materials with multiple phases includes the solid-state phase transformation methods such as precipitation, separation, and eutectic transformation. In PbTe-based TE alloys, this approach has been widely used with decomposition during the cooling process and resulted in the formation of nanocomposites with uniformly distributed nanoinclusions [12,13]. Recently, several studies for the preparation of bulk-type materials with multiple phases have been reported in La-, Ce-, and Yb-filled skutterudites mainly due to the uneven distribution of cations [14–18].

Here we provide a rapid solidification process (RSP)-based synthesis route to prepare submicron-scale heterograin structure of *p*-type Yb-filled $(Fe,Co)_4Sb_{12}$ skutterudites since RSP can trigger the generation of non-equilibrium or supersaturated phases due to high quenching speed. In this study, we used a melt spinning (MS) process, in which cooling rates are in the range of 10^4–10^7 K s^{-1}.

Mixed grains of $Yb_xFe_{3-y}Co_{1+y}Sb_{12}$ and $Yb_zFe_{3+y}Co_{1-y}Sb_{12}$ were formed in melt spun ribbons, and this heterograin structure was maintained in the compacted bulks. A high power factor of ~3.13 mW m^{-1} K^{-2} and a low κ_{lat} of ~1.14 W m^{-1} K^{-1} were observed at 700 K in $Yb_{0.85}Fe_3CoSb_{12}$ (nominal composition) in the presence of an interface between two different grains. A peak zT value of 0.66 at 700 K was obtained.

2. Materials and Methods

Ingots of $Yb_xFe_3CoSb_{12}$ (x = 0.80, 0.85, 0.90) were prepared by melting and solidification. Mixtures of high purity (>99.99%) elements of Yb, Fe, Co, and Sb with targeted compositions were melted at 1373 K for 12 h in a vacuum (at 2.0×10^{-2} Pa) sealed quartz tube (15 mm in diameter; inside wall was coated with carbon by acetone cracking). Acquired ingots were crushed into chunks (~3 mm), and then the ribbons (1–1.5 mm wide, 10–15 mm long, and 10–12 μm thick) were fabricated by using the melt spinning (MS) process. The MS equipment consists of an induction heater, a gas control system, a graphite nozzle (~0.5 mm), and a Cu wheel (250 mm in diameter). The crushed chunks (~7 g) of ingot were melted in a graphite nozzle by induction heating, and molten alloy was injected onto a rotating Cu wheel (~3600 rpm). The ribbons were pulverized into powders in an agate mortar, and compacted bulks (10 mm in diameter and 3 mm in thickness) were fabricated by using spark plasma sintering (SPS, SPS-630lx, Fuji Electronic Industrial, Saitama, Japan) at 823 K for 3 min under a uniaxial pressure of 45 MPa.

Phase formation behaviors of the melt spun ribbons and SPSed bulks were analyzed by the X-ray diffraction (XRD) method (EMPYRENA diffractometer, PANalytical B.V., The Netherlands) with Cu $K_{\alpha 1}$ radiation. The microstructures of the samples were confirmed by field emission scanning electron microscopy (FESEM, JSM-7500F, JEOL, Tokyo, Japan). In order to determine the zT values of the SPSed bulks, we evaluated the temperature dependences of σ and S by commercial equipment (ZEM-3, ULVAC, Chigasaki, Japan). The temperature dependence of κ ($=C_p \times \rho \times \lambda$) was calculated from a separate measurement of the heat capacity (C_p), density (ρ), and thermal diffusivity (λ). The C_p values were measured by using differential scanning calorimetry (DSC 200 F3 Maia, NETZSCH, Selb, Germany) and λ values were measured by using a laser flash apparatus (LFA467, NETZSCH, Selb, Germany) from 300 K to 700 K. In order to evaluate the electronic and thermal transport parameters, we also

obtained the carrier concentration (n_c) and Hall mobility (μ_{Hall}) at 300 K by using a Hall measurement system (HMS-3000, Ecopia, Chandler Heights, AZ, USA) with a van der Pauw configuration.

3. Results and Discussion

By using the MS process, we attempted to generate *p*-type Yb-filled $(Fe,Co)_4Sb_{12}$ skutterudites with multiple phases. Figure 1a shows the XRD analysis results for the melt spun ribbons of $Yb_{0.9}Fe_3CoSb_{12}$ (starting nominal composition). The melt spun ribbons of $Yb_{0.9}Fe_3CoSb_{12}$ contain multiple secondary phases including $FeSb_2$, CoSb, $YbSb_2$, and Sb. It should be noted that two phases of $CoSb_3$-based alloys (skutterudites) with different lattice constants were detected. Figure 1b shows the XRD patterns of SPSed $Yb_xFe_3CoSb_{12}$ (x = 0.85, 0.90) bulks. Yb-filled skutterudites without any impurities were successfully fabricated, benefitting from the activated phase evolution during SPS due to the homogenous dispersion of various nanoscale phases in the ribbons (the sizes of grains (Yb filled Fe_3CoSb_{12}, $FeSb_2$, CoSb, $YbSb_2$, and Sb ranged from 50 nm to 100 nm, as shown in SEM image (Figure 2a) of the contact surface of melt spun ribbon of $Yb_{0.85}Fe_3CoSb_{12}$, which triggers the diffusion of ions during the sintering process) [19–21], while two different Yb-filled skutterudites found in melt spun ribbons still remained in SPSed bulks. Distinct left shoulders (red arrows in Figure 1b) can be seen in all XRD peaks of $Yb_{0.85}Fe_3CoSb_{12}$, and separated smaller XRD peaks (blue arrows in Figure 1b) of the (0 3 1) and (1 3 2) reflections are clearly observed in $Yb_{0.9}Fe_3CoSb_{12}$. These results suggest that a composite of two different skuttrudites was generated by MS and SPS due to uneven distribution of cations, and the formation of two different filled skutterudites has been reported previously [14–18]. The calculated lattice constants of the majority skutterudite (9.0820(1) Å for $Yb_{0.85}Fe_3CoSb_{12}$ and 9.0881(7) Å for $Yb_{0.9}Fe_3CoSb_{12}$) are smaller than those of the minority skutterudite (9.1659(5) Å for $Yb_{0.85}Fe_3CoSb_{12}$ and 9.2037(9) Å for $Yb_{0.9}Fe_3CoSb_{12}$), indicating that the compositions of the composite are $Yb_xFe_{3-y}Co_{1+y}Sb_{12}$ (Co-rich skutterudite) and $Yb_zFe_{3+y}Co_{1-y}Sb_{12}$ (Fe-rich skutterudite), related with the size difference between Fe^{2+} (CN = 6, 0.61 Å) and Co^{3+} (CN = 6, 0.55 Å) [22]. In addition, the lattice constants of $Yb_xFe_{3-y}Co_{1+y}Sb_{12}$ are almost the same, while those of $Yb_zFe_{3+y}Co_{1-y}Sb_{12}$ increase gradually with Yb content due to the charge stability in *p*-type skutterudites.

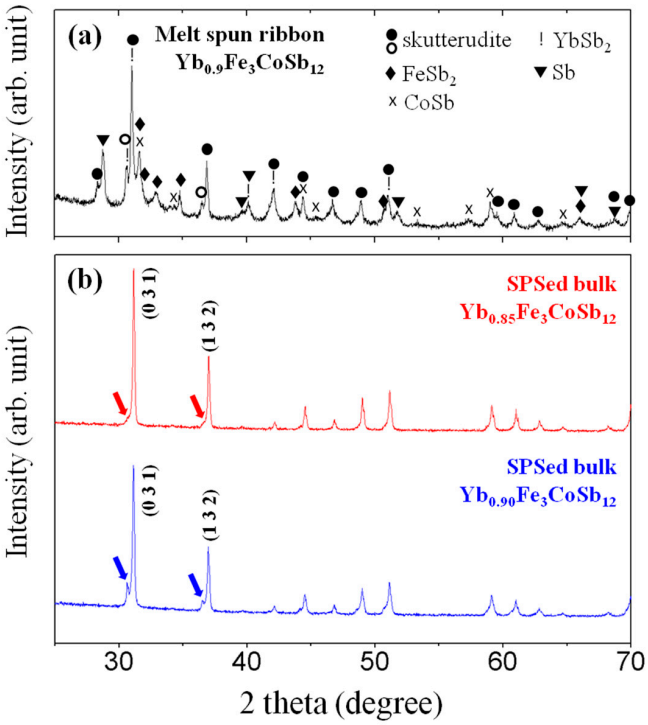

Figure 1. (**a**) X-ray diffraction (XRD) pattern for the melt spun ribbons of $Yb_{0.90}Fe_3CoSb_{12}$ and (**b**) XRD patterns for the SPSed bulks of $Yb_{0.85}Fe_3CoSb_{12}$ and $Yb_{0.90}Fe_3CoSb_{12}$.

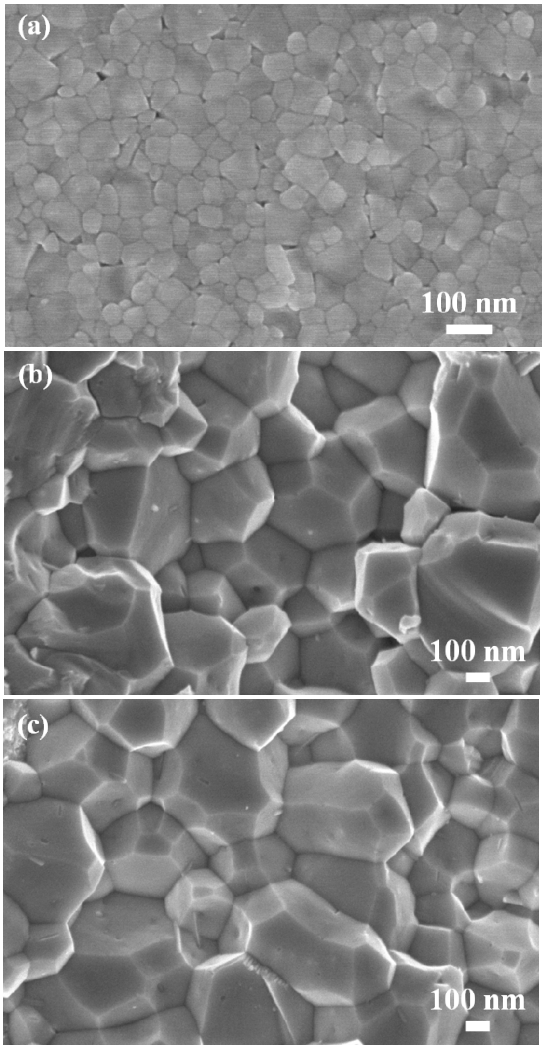

Figure 2. (**a**) Scanning electron microscopy (SEM) image for the contact surface of melt spun ribbon of $Yb_{0.85}Fe_3CoSb_{12}$; and SEM images for the fractured surfaces of SPSed, (**b**) $Yb_{0.85}Fe_3CoSb_{12}$ and (**c**) $Yb_{0.90}Fe_3CoSb_{12}$ bulks.

Figure 2b,c shows SEM images of the fractured surface of SPSed bulks of $Yb_{0.85}Fe_3CoSb_{12}$ and $Yb_{0.9}Fe_3CoSb_{12}$ with ~500 nm average grain size. It is noted that features of nano-scale inclusions are not observed, indicating that a submicron-scale heterograin structure is fabricated in compacted bulks.

Figure 3a shows the temperature-dependent σ and S of SPSed $Yb_xFe_3CoSb_{12}$ (x = 0.80, 0.85, 0.90) bulks, respectively. All S values were found to be positive, confirming p-type semiconducting characteristics. Both the σ and S values slightly increase with Yb content within the entire measured temperature range, and enhanced power factor ($S^2\sigma$) values were obtained at higher Yb content (x = 0.85 and 0.90), as shown in Figure 3b. To clarify this, we obtained the n_c and μ_{Hall} at 300 K form Hall measurement and also calculated the density of states (DOS) effective mass (m_d*) by the following Equation (2) [2]:

$$S = \frac{8\pi^2 {k_B}^2}{3eh^2}\left(\frac{\pi}{3n_c}\right)^{2/3} m_d^* T, \quad (2)$$

where k_B is the Boltzmann constant, and h is the Planck constant, respectively. As shown in Figure 3c, the n_c values increase with Yb content, which is further experimental evidence for the generation of a heterograin structure. Since the Fe atom has one electron less than the Co atom ($Fe_{Co}^{/}$), the increase in n_c is considered to be related with the formation of Fe-rich skutterudite. By the energy filtering effect originating from the difference in band gap between heterograins, m_d* values increase with Yb

content (inset of Figure 3b). However, μ_{Hall} values decrease with Yb content, mainly due to the carrier scattering at the interface between $Yb_xFe_{3-y}Co_{1+y}Sb_{12}$ and $Yb_zFe_{3+y}Co_{1-y}Sb_{12}$ grains (Figure 3c). Related with this trade-off relationship between m_d* and μ_{Hall}, a maximum power factor value of ~3.13 mW m^{-1} K^{-2} is obtained in $Yb_{0.85}Fe_3CoSb_{12}$, benefitting from the formation of a heterograin structure with optimized band alignment.

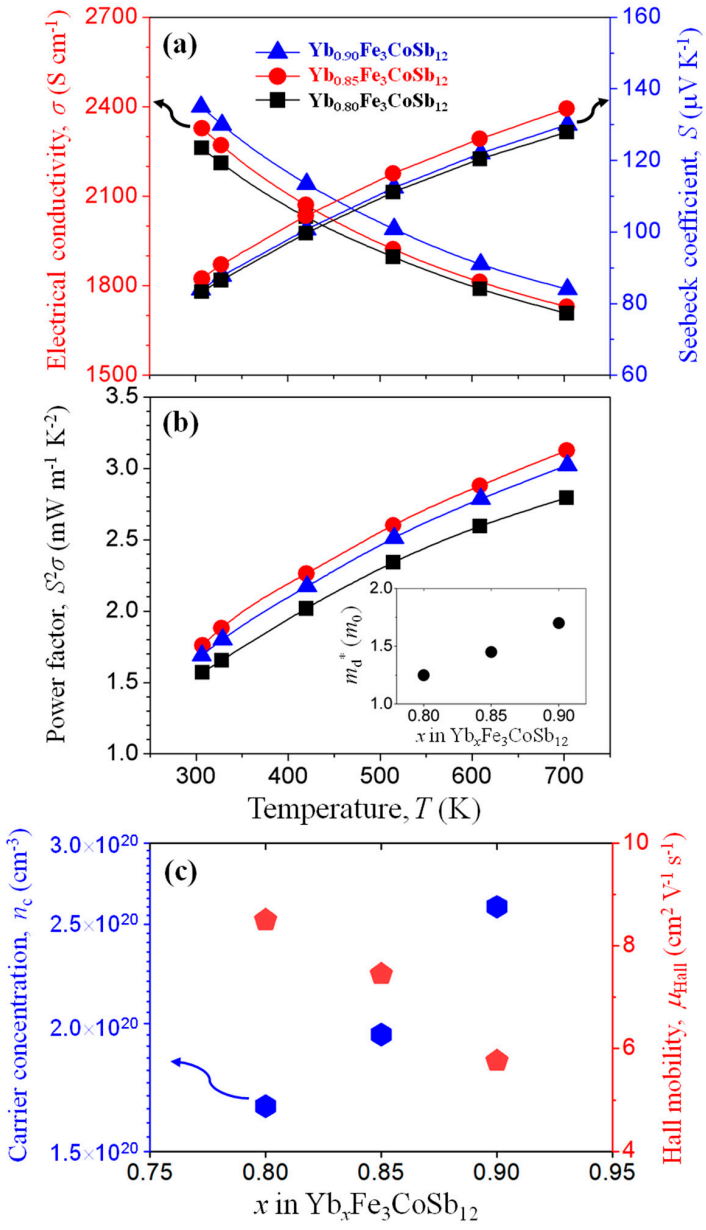

Figure 3. Temperature dependences of (**a**) electrical conductivity (σ), Seebeck coefficient (S) and (**b**) power factor (σS^2) for $Yb_xFe_3CoSb_{12}$ (x = 0.80, 0.85, 0.90) bulks. Density of states effective mass (m_d*) values are shown in the inset of (**b**). (**c**) Room temperature carrier concentration (n_c) and Hall mobility (μ_{Hall}) for $Yb_xFe_3CoSb_{12}$ (x = 0.80, 0.85, 0.90) bulks.

We also elucidate the effect of the heterograin structure on the thermal transport properties of *p*-type Yb-filled skutterudites. As shown in Figure 4a, κ values of $Yb_{0.90}Fe_3CoSb_{12}$ are rather lower compared to those of $Yb_{0.80}Fe_3CoSb_{12}$, despite higher σ values. We calculated the temperature-dependent κ_{lat} values with Yb content (Figure 4b) from measured κ and estimated κ_{ele} (inset of Figure 4b) by the Wiedemann-Frantz law ($\kappa_{ele} = L\sigma T$, where L is Lorentz number).

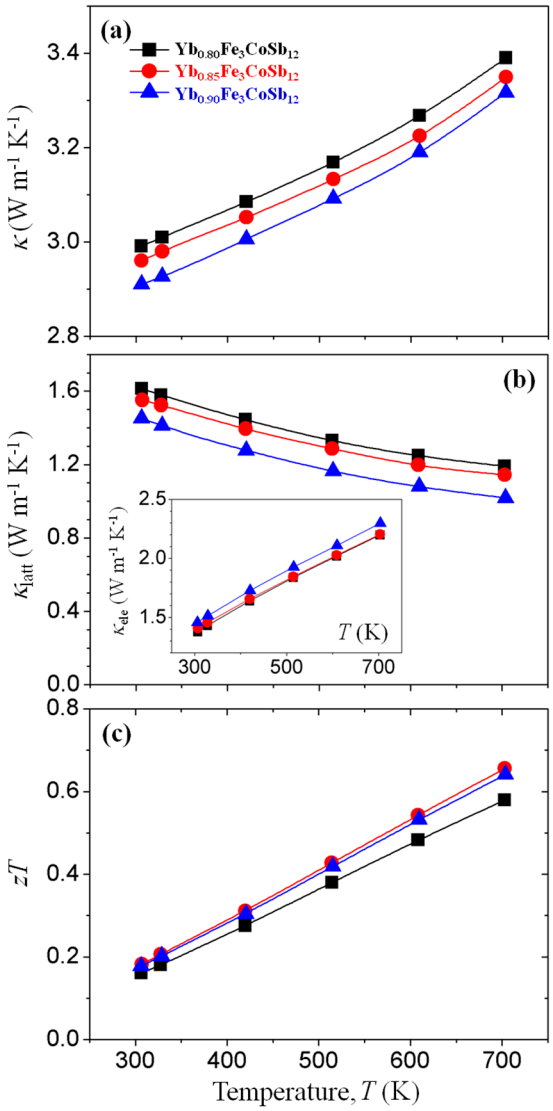

Figure 4. Temperature dependences of (**a**) total thermal conductivity (κ) and (**b**) lattice thermal conductivity (κ_{lat}) for $Yb_xFe_3CoSb_{12}$ (x = 0.80, 0.85, 0.90) bulks. Electronic contribution for the thermal conduction (κ_{ele}) is shown in the inset of (**b**). (**c**) Temperature dependences of dimensionless figure of merit (zT) for $Yb_xFe_3CoSb_{12}$ (x = 0.80, 0.85, 0.90) bulks.

Assuming that the acoustic phonon scattering mechanism is dominant, temperature-dependent L values are calculated by the following Equation (3) [23]:

$$L = 1.5 + Exp[-\frac{|S|}{116}]. \quad (3)$$

The L values ranged from 1.814 to 1.988 W Ω K^{-2} for all samples. The κ_{lat} values almost proportionally decrease with temperature, suggesting that the effect of the bipolar contribution (κ_{bp}) on thermal conduction is negligible even at higher temperatures. A temperature-independent vibrational mode in *p*-type La-filled Fe_3CoSb_{12} [24] is not found in this Yb-filled $(Fe,Co)_4Sb_{12}$ system. This difference in thermal conduction behavior might originate from the variable charge state of Yb ions. Resultantly, κ_{lat} values decrease with Yb content within the entire measured temperature range due to the intensified rattling effect and mismatched phonon modes at the interface between heterograins. Low κ_{lat} values of 1.55 W m^{-1} K^{-1} at 300 K and 1.14 W m^{-1} K^{-1} at 700 K were observed in $Yb_{0.85}Fe_3CoSb_{12}$. Temperature dependence of zT is shown in Figure 4c. A peak zT of 0.66 was

obtained at 700 K for $Yb_{0.85}Fe_3CoSb_{12}$ due to the enhanced power factor and simultaneously reduced κ_{lat}, thus demonstrating that heterograin structuring is a promising approach to improve the zT of filled skutterudites.

4. Conclusions

We fabricated *p*-type Yb-filled $(Fe,Co)_4Sb_{12}$ skutterudites with micro-scale heterograins by using a combined technique of melt spinning and spark plasma sintering. By the in-situ generation of interfaces between Fe-rich and Co-rich grains, which act as both an energy barrier for carrier transport and a scattering center for phonon transport, the power factor was enhanced due to the formation of an energy barrier for carrier transport, and the lattice thermal conductivity was reduced due to intensified boundary phonon scattering. This approach to prepare heterograin structured thermoelectric materials provides progress in both the facile process that is suggested and the fundamentals of defect engineered materials for enhancing thermoelectric performance.

Author Contributions: Data curation, K.H.L. and S.H.B.; Formal analysis, S.-M.C.; Investigation, K.H.L. and S.H.B.; Methodology, K.H.L. and S.H.B.; Supervision, S.-M.C.; Writing—original draft, K.H.L. and S.H.B.; Writing—review & editing, S.-M.C. All authors have read and agreed to the published version of the manuscript.

Funding: This research was supported by the Basic Science Research Program (NRF-2017R1D1A1A09000570) and by a grant from the Industrial Core Technology Development Program (10083640). This research was also supported by Low-dimensional Materials Genome Development by Korea Research Institute of Standards and Science (KRISS—2018—18011084). This paper was partially supported by the Graduate School Research Program of KOREATECH. And thanks the Cooperative Equipment Center at KOREATECH for assistance with SEM XRD analysis.

Conflicts of Interest: The authors declare no conflict of interest.

References

1. Sales, B.C.; Mandrus, D.; Williams, R.K. Filled Skutterudite Antimonides: A New Class of Thermoelectric Materials. *Science* **1996**, *272*, 1325–1328. [CrossRef] [PubMed]
2. Snyder, G.J.; Toberer, E.S. Complex thermoelectric materials. *Nat. Mater.* **2008**, *7*, 105–114. [CrossRef] [PubMed]
3. Schierning, G.; Chavez, R.; Schmechel, R.; Balke, B.; Rogl, G.; Rogl, P. Concepts for medium-high to high temperature thermoelectric heat-to-electricity conversion: A review of selected materials and basic considerations of module design. *Transl. Mater. Res.* **2015**, *2*, 025001. [CrossRef]
4. Cai, B.; Hu, H.; Zhuang, H.L.; Li, J.F. Promising materials for thermoelectric applications. *J. Alloy. Compd.* **2019**, *806*, 471–486. [CrossRef]
5. Shi, X.; Kong, H.; Li, C.P.; Uher, C.; Yang, J.; Salvador, J.R.; Wang, H.; Chen, L.; Zhang, W. Low thermal conductivity and high thermoelectric figure of merit in n-type $Ba_xYb_yCo_4Sb_{12}$ $Ba_xYb_yCo_4Sb_{12}$ double-filled skutterudites. *Appl. Phys. Lett.* **2008**, *92*, 182101. [CrossRef]
6. Ballikaya, S.; Uzar, N.; Yildirim, S.; Salvador, J.R.; Uher, C. High thermoelectric performance of In, Yb, Ce multiple filled $CoSb_3$ based skutterudite compounds. *J. Solid State Chem.* **2012**, *193*, 31–35. [CrossRef]
7. Shi, X.; Yang, J.; Salvador, J.R.; Chi, M.; Cho, J.Y.; Wang, H.; Bai, S.; Yang, J.; Zhang, W.; Chen, L. Multiple-Filled Skutterudites: High Thermoelectric Figure of Merit through Separately Optimizing Electrical and Thermal Transports. *J. Am. Chem. Soc.* **2011**, *133*, 7837–7846. [CrossRef]
8. Mun, H.; Choi, S.M.; Lee, K.H.; Kim, S.W. Boundary Engineering for the Thermoelectric Performance of Bulk Alloys Based on Bismuth Telluride. *ChemSusChem* **2015**, *8*, 2312–2326. [CrossRef]
9. Heinz, N.A.; Ikeda, T.; Pei, Y.; Snyder, G.J. Applying Quantitative Microstructure Control in Advanced Functional Composites. *Adv. Funct. Mater.* **2014**, *24*, 2135–2153. [CrossRef]
10. Rogl, G.; Bursik, J.; Grytsiv, A.; Puchegger, S.; Soprunyuk, V.; Schranz, W.; Yan, X.; Bauer, E.; Rogl, P. Nanostructuring as a tool to adjust thermal expansion in high ZT skutterudites. *Acta Mater.* **2018**, *145*, 359–368. [CrossRef]
11. Zhou, Z.; Li, J.; Fan, Y.; Zhang, Q.; Lu, X.; Fan, S.; Kikuchi, K.; Nomura, N.; Kawasaki, A.; Wang, L.; et al. Uniform dispersion of SiC in Yb-filled skutterudite nanocomposites with high thermoelectric and mechanical performance. *Scr. Mater.* **2019**, *162*, 166–171. [CrossRef]

12. Biswas, K.; He, J.; Zhang, Q.; Wang, G.; Uher, C.; Dravid, V.P.; Kanatzidis, M.G. Strained endotaxial nanostructures with high thermoelectric figure of merit. *Nat. Chem.* **2011**, *3*, 160–166. [CrossRef] [PubMed]
13. Biswas, K.; He, J.; Blum, I.D.; Wu, C.; Hogan, T.P.; Seidman, D.N.; Dravid, V.P.; Kanatzidis, M.G. High-performance bulk thermoelectrics with all-scale hierarchical architectures. *Nature* **2012**, *489*, 414–418. [CrossRef] [PubMed]
14. Wei, R.; Huiyuan, G.; Zihao, Z.; Lixia, Z. Filling-Fraction Fluctuation Leading to Glasslike Ultralow Thermal Conductivity in Caged Skutterudites. *Phys. Rev. Lett.* **2017**, *118*, 245901. [CrossRef]
15. Ren, W.; Geng, H.; Zhang, L.; Liu, X.; He, T.; Feng, J. Simultaneous blocking of minority carrier and high energy phonon in p-type skutterudites. *Nano Energy* **2018**, *46*, 249–256. [CrossRef]
16. Serrano-Sánchez, F.; Prado-Gonjal, J.; Nemes, N.M.; Biskup, N.; Varela, M.; Dura, O.J.; Martínez, J.L.; Fernández-Díaz, M.T.; Fauth, F.; Alonso, J.A. Low thermal conductivity in La-filled cobalt antimonide skutterudites with an inhomogeneous filling factor prepared under high-pressure conditions. *J. Mater. Chem. A* **2018**, *6*, 118–126. [CrossRef]
17. Serrano-Sánchez, F.; Prado-Gonjal, J.; Nemes, N.M.; Biskup, N.; Dura, O.J.; Martínez, J.L.; Fernández-Díaz, M.T.; Fauth, F.; Alonso, J.A. Thermal Conductivity Reduction by Fluctuation of the Filling Fraction in Filled Cobalt Antimonide Skutterudite Thermoelectrics. *ACS Appl. Energy Mater.* **2018**, *1*, 6181–6189. [CrossRef]
18. Gainza, J.; Serrano-Sánchez, F.; Prado-Gonjal, J.; Nemes, N.M.; Biskup, N.; Dura, O.J.; Martínez, J.L.; Fauth, F.; Alonso, J.A. Substantial thermal conductivity reduction in mischmetal skutterudites $Mm_xCo_4Sb_{12}$ prepared under high-pressure conditions due to uneven distribution of the rare-earth elements. *J. Mater. Chem. C* **2019**, *7*, 4124–4131. [CrossRef]
19. Li, H.; Tang, X.; Zhang, Q.; Uher, C. Rapid preparation method of bulk nanostructured $Yb_{0.3}Co_4Sb_{12+y}$ compounds and their improved thermoelectric performance. *Appl. Phys. Lett.* **2008**, *93*, 252109. [CrossRef]
20. Tan, G.; Liu, W.; Wang, S.; Yan, Y.; Li, H.; Tang, X.; Uher, C. Rapid preparation of $CeFe_4Sb_{12}$ skutterudite by melt spinning: Rich nanostructures and high thermoelectric performance. *J. Mater. Chem. A* **2013**, *1*, 12657–12668. [CrossRef]
21. Lee, S.; Lee, K.H.; Kim, Y.M.; Kim, H.S.; Snyder, G.J.; Baik, S.; Kim, S.W. Simple and efficient synthesis of nanograin structured single phase filled skutterudite for high thermoelectric performance. *Acta Mater.* **2018**, *142*, 8–17. [CrossRef]
22. Tang, X.; Zhang, Q.; Chen, L.; Goto, T.; Hirai, T. Synthesis and thermoelectric properties of p-type- and n-type-filled skutterudite $R_yM_xCo_{4-x}Sb_{12}$ (R:Ce,Ba,Y;M:Fe,Ni). *J. Appl. Phys.* **2005**, *97*, 093712. [CrossRef]
23. Kim, H.S.; Gibbs, Z.M.; Tang, Y.; Wang, H.; Snyder, G.J. Characterization of Lorenz number with Seebeck coefficient measurement. *APL Mater.* **2015**, *3*, 041506. [CrossRef]
24. Son, G.; Lee, K.H.; Park, H.W.; Caron AKim, I.H.; Lee, S.; Choi, S.M. Control of electrical to thermal conductivity ratio for p-type $La_xFe_3CoSb_{12}$ thermoelectrics by using a melt-spinning process. *J. Alloys Compd.* **2017**, *729*, 1209–1214. [CrossRef]